

# Correlation between tunneling magnetoresistance and magnetization in dipolar-coupled nanoparticle arrays

D. Kechrakos\* and K. N. Trohidou

*Institute of Materials Science, NCSR Demokritos, 15310 Athens, Greece*

(Received 30 July 2004; revised manuscript received 5 November 2004; published 23 February 2005)

The tunneling magnetoresistance (TMR) of a hexagonal array of dipolar-coupled anisotropic magnetic nanoparticles is studied using a resistor network model and a realistic micromagnetic configuration obtained by Monte Carlo simulations. Analysis of the field-dependent TMR and the corresponding magnetization curve shows that dipolar interactions suppress the maximum TMR effect, increase or decrease the field sensitivity depending on the direction of applied field, and introduce strong dependence of the TMR on the direction of the applied magnetic field. For off-plane magnetic fields, maximum values in the TMR signal are associated with the critical field for irreversible rotation of the magnetization. This behavior is more pronounced in strongly interacting systems (magnetically soft), while for weakly interacting systems (magnetically hard) the maximum of TMR ( $H_{max}$ ) occurs below the coercive field ( $H_c$ ), in contrast to the situation for noninteracting nanoparticles ( $H_c=H_{max}$ ) or in-plane fields. The relation of our simulations to recent TMR measurements in self-assembled Co nanoparticle arrays is discussed.

DOI: 10.1103/PhysRevB.71.054416

PACS number(s): 75.50.Tt, 75.47.-m, 75.75.+a, 75.60.Ej

## I. INTRODUCTION

Intense research activity in the magnetic properties of ordered nanoparticle arrays<sup>1-3</sup> is motivated on one hand by the potential of these materials in advancing the magnetic storage density limit to the range of 1 Tb/in<sup>2</sup>, and on the other hand by basic scientific interest to reveal the underlying mechanism of magnetization reversal in a collection of interacting magnetic nanoparticles. The hexagonal arrangement of self-assembled nanoparticle arrays rules out the complications introduced by positional randomness in other nanoparticle-based systems (ferrofluids, granular metals) and makes the theoretical analysis simpler. The investigation of the hysteretic behavior and the underlying magnetization reversal mechanism in nanoparticle arrays is a central issue in the research effort on magnetic nanoparticle arrays. The requirements for high packing densities inevitably introduce a new aspect in the magnetization dynamics of these assemblies, namely, the collective behavior caused by particle interactions. The insulating nature of the surrounding the nanoparticle material rules out any type of exchange forces between them, because it prevents electron transfer between neighboring nanoparticles. On the other hand, magnetostatic interactions are always present and their effects have been frequently demonstrated in experiments on self-assembled arrays. In particular, reduction of the remanence at low temperature,<sup>4</sup> increase of the blocking temperature,<sup>5-7</sup> increase of the barrier distribution width,<sup>8</sup> deviations of the zero-field cooled magnetization curves from the Curie behavior,<sup>3</sup> difference between the in-plane and normal-to-plane remanence,<sup>9</sup> and increase of the blocking temperature with frequency of applied field<sup>10</sup> have been observed and attributed to interparticle magnetostatic interactions. In addition to the experimental work, various numerical studies that focused on the ground state configuration and the hysteresis behavior of dipolar interacting nanoparticle arrays have appeared. The interplay of dipolar interactions and perpendicu-

lar anisotropy was shown<sup>11</sup> to induce a reorientation transition below a critical temperature and interaction-induced shape anisotropy of a finite sample controls the magnetization reversal mode. Dipolar interactions were found to decrease the coercive field of magnetic nanoparticle arrays independently of the array topology (square or hexagonal) despite the fact that the ground state configuration is determined by the array topology.<sup>12</sup> The presence of an incomplete second layer with hexagonal structure does not destroy the ferromagnetic (FM) ordering of the ground state,<sup>13</sup> while even slight structural disorder within the array destroys that ordering.<sup>14</sup> On the other hand, higher order (quadropolar) magnetostatic interactions were shown to stabilize the long range order of the ground state in a nanoparticle array.<sup>15</sup>

Although great theoretical and experimental effort has been made towards the understanding of the magnetic properties of self-assembled nanoparticle arrays, very little work has been done on electronic transport in these systems. In a recent work, Black *et al.*<sup>2</sup> demonstrated that the conductivity of a Co nanoparticle self-assembled film is dominated by spin-dependent tunneling, which leads to large ( $\sim 10\%$ ) tunneling magnetoresistance (TMR) values at low temperature ( $\sim 20$  K). In these experiments, a TMR signal with rich structure was observed, which was attributed to the details of the underlying magnetization reversal mechanism. Spin-dependent transport measurements have been previously used as an indirect probe of the micromagnetic structure in spin valves,<sup>16</sup> magnetic tunnel junctions,<sup>17</sup> artificial ferromagnetic layers,<sup>18</sup> and ferromagnetic rings.<sup>19</sup> The basic idea behind these experiments is that the spin-dependent scattering mechanism leads to a resistivity proportional to the (average) relative orientation of the magnetic moments of separated magnetic regions (either nanoparticles or magnetic domains with different magnetization orientation). Thus, resistivity measurements could in principle reveal the underlying magnetic correlations. Indeed, in the above-mentioned experiments,<sup>16-19</sup> the underlying micromagnetic structure

was efficiently correlated to the magnetoresistance signal. Resistor network (RN) models have been implemented in the interpretation of magnetoresistance measurements in the above-mentioned experiments<sup>16,18</sup> and earlier experiments in magnetic granular films.<sup>20–22</sup> More recently, Inoue and Maekawa<sup>23</sup> have introduced a RN model that interpreted the weak temperature-dependent TMR in Co-Al-O granular films. The Inoue-Maekawa model combined the ideas of Helman and Abeles<sup>21</sup> on the electron hopping mechanism in granular metals, according to which the intergranular conductivity decays proportionally to the intergranular distance with the model of Julliere<sup>24</sup> on spin-dependent transport in is proportionally to the relative orientation of the magnetizations in the FM layers.

In conductivity measurements in self-assembled Co nanoparticle arrays,<sup>2</sup> an exponential temperature dependence  $\ln G \sim -T^{-1}$  was found, which is characteristic of a thermally activated tunneling (hopping) process between nanoparticles with negligible size dispersion. Furthermore, contributions to the electric current from a cotunneling process were ruled out.<sup>2</sup> Based on these conclusions, we suggest that a RN composed of resistors defined according to the Inoue-Maekawa model would be appropriate to study charge transport in self-assembled magnetic nanoparticle arrays.

In this paper, we study by numerical simulations the correlations between the micromagnetic structure of hexagonal arrays of dipolar interacting nanoparticles and the tunneling magnetoresistance of the sample. To this end, Monte Carlo (MC) simulations of the magnetic configuration at a finite temperature and applied field are performed. The conductivity of the sample is obtained, at equilibrium, by numerical solution of a RN model which incorporates the detailed magnetic configuration.

The remainder of the paper is organized as follows. In Sec. II, we describe the model of the magnetic structure and the method of simulation. The RN model is also described in that section. In Sec. III, we present numerical results and discuss the dependence of the TMR on the applied field, the interparticle distance, and the direction of applied field. A discussion of our results and a summary of this work are given in Sec. IV.

## II. THE MODEL AND THE SIMULATION METHOD

Let us consider  $N$  identical spherical particles with diameter  $D$  forming a two-dimensional triangular lattice in the  $xy$  plane with lattice constant  $d \geq D$ . The size dispersion of the nanoparticles can be neglected to a good approximation, as for self-assembled samples a very narrow size distribution ( $\sigma \approx 5\%$ ) has been achieved.<sup>2</sup> The particles are single domain, with uniaxial anisotropy in a random direction, and they interact via dipolar forces. The total energy of the system is given as

$$E = g \sum_i \frac{(\hat{S}_i \cdot \hat{S}_j) - 3(\hat{S}_i \cdot \hat{R}_{ij})(\hat{S}_j \cdot \hat{R}_{ij})}{(R_{ij}/d)^3} - k \sum_i (\hat{S}_i \cdot \hat{e}_i)^2 - h \sum_i (\hat{S}_i \cdot \hat{H}), \quad (1)$$

where  $\hat{S}_i$  is the magnetic moment direction (spin) of particle

$i$ ,  $\hat{e}_i$  is the easy-axis direction, and  $R_{ij}$  is the center-to-center distance between particles  $i$  and  $j$ . Hats indicate unit vectors. The energy parameters entering Eq. (1) are the dipolar energy  $g = \mu^2/d^3$ , where  $\mu = M_s V$  is the particle moment, the anisotropy energy  $k = K_1 V$ , and the Zeeman energy  $h = \mu H$  due to the applied field  $H$ . The relative strength of the energy parameters entering Eq. (1), the thermal energy  $t = k_B T$ , and the treatment history of the sample determine the micromagnetic configuration. However, the transition from single-particle to collective behavior is determined solely by the ratio of the dipolar to the anisotropy energy  $g/k = (\pi/2) \times (M_s^2/K_1)(D/d)^3$ . The reported values<sup>3,5,9,10</sup> for fcc or hcp Co nanoparticles are  $g/k \sim 0.2 - 0.4(D/d)^3$ , while for the soft  $\varepsilon$ -Co phase, higher values are expected.<sup>3</sup> These values define the range of parameters to be used further on in our simulations.

The magnetic configuration of the nanoparticle ensemble under an applied field  $H$  and finite temperature  $T$  was obtained by a MC simulation, using the standard Metropolis algorithm.<sup>25</sup> At a given temperature and applied field, the system was allowed to relax towards equilibrium using  $10^3$  MC steps per spin, and thermal averages were calculated over the subsequent  $10^4$  steps. The results were averaged over 2–10 independent random number sequences corresponding to different realizations of thermal fluctuations. Simulations were performed on a rectangular  $L_x \times L_y$  simulation cell with  $L_x/d = 16$  and  $L_y/d = 8\sqrt{3}$ . For the simulations of the magnetic structure, we used free boundaries in the  $z$  axis and periodic boundaries in the  $xy$  plane to avoid undesirable demagnetizing effects due to free poles at the sample boundaries. The dipolar interactions were summed to infinite order in-plane, using the Ewald summation method for a quasi-two-dimensional system.<sup>26</sup>

We proceed with the description of the RN model employed to study the TMR. For a given micromagnetic configuration  $\{\hat{S}_i\}$  of the nanoparticle array, we define the conductivity between two nanoparticles  $i$  and  $j$  as<sup>2,23</sup>

$$\sigma_{ij} = \sigma_0 (1 + P^2 \cos \theta_{ij}) \exp(-R_{ij}/a - E_c/k_B T), \quad (2)$$

where  $\sigma_0 = 2e^2/h$  is the conductivity quantum,  $P$  is the spin polarization of the conduction electrons,  $\cos \theta_{ij} = (\hat{S}_i \cdot \hat{S}_j)$ ,  $E_c = e^2/2C$  is the activation energy to charge a neutral nanoparticle by addition of a single electron,  $C$  is the nanoparticle capacitance relative to its surrounding medium, and  $a = \hbar/\sqrt{8m^*(U-E_F)}$  is the decay length of the electron wave function in the insulating barrier of height  $U$  relative to the Fermi energy. In all our simulations we assumed  $a=d$ , as a sufficient requirement to allow charge transfer between neighboring nanoparticles and  $P=0.34$  as an appropriate value for Co nanoparticles.<sup>2,27</sup> As shown by Inoue and Maekawa,<sup>23</sup> consideration of the change in magnetic energy of nanoparticles due to tunneling of carriers leads to an *increase* of the global resistance with applied field and it also has a negligibly small contribution for Co nanoparticles at temperatures above  $T \approx 3$  K. Since transport measurements in Co nanoparticle arrays<sup>2</sup> were performed at 4.5 K, we expect that the change in magnetic energy is not important, and it has been neglected in Eq. (2).

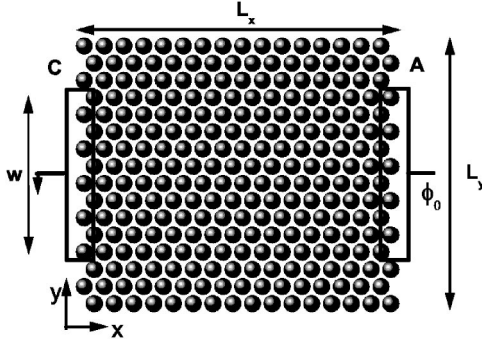


FIG. 1. Sketch of the nanoparticle array used in our simulations with attached electrodes (C, A) on opposite boundaries along the  $x$  axis. The width of the electrodes shown is  $w=10(d\sqrt{3}/2)$ , and they are coupled only to the outermost nanoparticle of each row.

Charge conservation on every node of the network implies

$$\sum_j \sigma_{ij}(\phi_i - \phi_j) = 0, \quad (3)$$

where  $\{\phi_i\}$  are the electric potentials. We consider two electrodes attached to the left (cathode) and right (anode) side of the sample along the  $x$  axis (Fig. 1). The width of the electrodes defines approximately the region of the sample through which the electric current flows and, consequently, the fraction of the nanoparticles that determine the thermal average value of TMR. In accordance with the experimental setup,<sup>2</sup> we have chosen  $w=10(d\sqrt{3}/2)$  for a sample with  $L_y = 16(d\sqrt{3}/2)$ . However, an increase of the electrode width up to  $w=L_y$ , did not modify our numerical results substantially, provided that demagnetizing effects due to free boundaries are negligible, namely, periodic boundaries are used and/or a small dipolar coupling strength ( $g/k \leq 0.2$ ) is assumed. Nanoparticles in contact with the electrodes share the same potential with them; thus, the boundary conditions are

$$\phi_i = 0; \quad i \in C \quad (4)$$

and

$$\phi_i = \phi_0; \quad i \in A, \quad (5)$$

where  $\phi_0$  is the voltage applied across the sample. The boundaries along the  $y$  axis are free, namely, there is no current flow across the  $y$ -axis boundary. The effective conductivity of the sample is obtained from the requirement that the total power consumption in the network must be equal to the sum of the power consumptions on all the resistors of the network.<sup>28</sup> Thus, the effective conductivity is given as

$$\sigma = \frac{1}{2\phi_0^2} \sum_{i,j} \sigma_{ij}(\phi_i - \phi_j)^2. \quad (6)$$

For simplicity, we have taken  $\phi_0=1$ ; in other words, all potentials  $\{\phi_i\}$  are scaled by the applied voltage. This assumption does not affect our results since the interparticle conductivities [Eq. (2)] are voltage independent (Ohmic regime). The set of  $N$  coupled linear equations in Eq. (3) with the boundary conditions given by Eqs. (4) and (5) are solved for

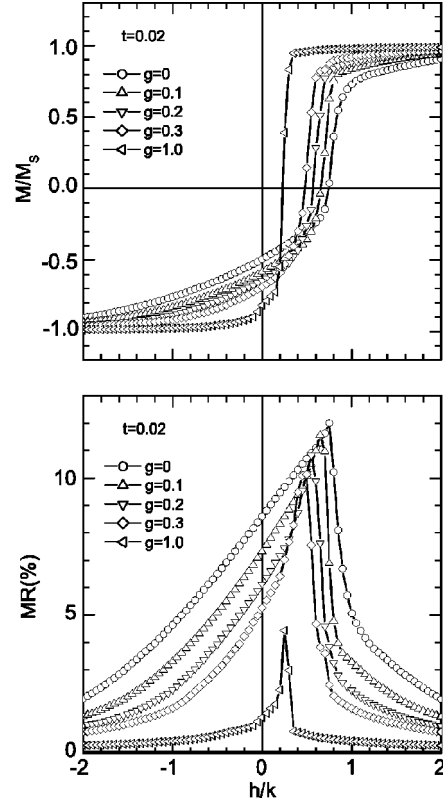


FIG. 2. Dependence of the low-temperature ( $t/k=0.02$ ) magnetization and TMR on the interparticle dipolar strength. The magnetic field is applied in-plane along the  $x$  axis. Only the lower hysteresis branch is shown.

the unknown potentials  $\{\phi_i\}$  by triangular decomposition<sup>29</sup> and the sample conductivity is obtained from Eq. (6). The result depends obviously of the magnetic configuration, which is used as input to obtain the interparticle conductivities [Eq. (2)]. Consequently, the sample conductivity depends on the applied magnetic field. A thermal average is obtained by averaging the conductivity values over a sequence of equilibrium spin configurations produced by the MC algorithm. Finally, the magnetoresistance of the sample is defined by

$$MR(H) = \frac{R(H) - R_s}{R_s} = \frac{\sigma_s - \sigma(H)}{\sigma(H)}, \quad (7)$$

where  $R_s$  and  $\sigma_s$  denote the saturation values of the resistivity and conductivity, respectively.

### III. NUMERICAL RESULTS

#### A. Dependence of magnetization and TMR on the dipolar strength

##### 1. In-plane magnetic field

We discuss first the variation of field-dependent TMR on the dipolar strength for an in-plane magnetic field. In Figs. 2 and 3 we show the lower branch of the hysteresis loop and the corresponding variation of TMR with applied field at a temperature below ( $t/k=0.02$ ) and above ( $t/k=0.15$ ) the

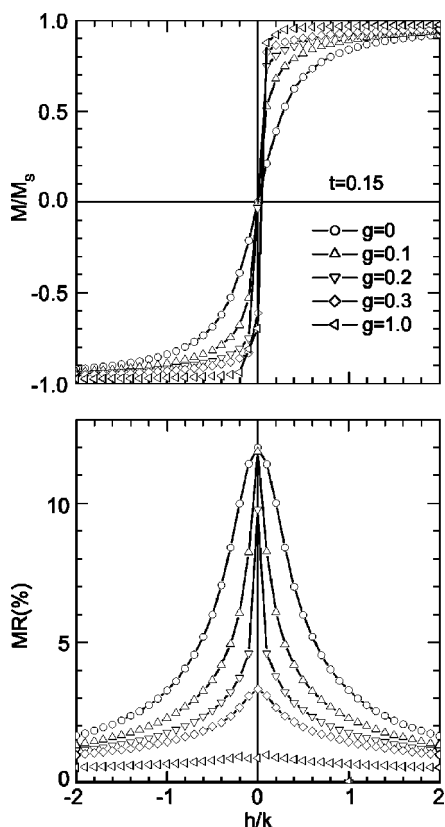


FIG. 3. Dependence of the high-temperature ( $t/k=0.15$ ) magnetization and TMR on the interparticle dipolar strength. The magnetic field is applied in-plane along the  $x$  axis. The blocking temperature for the noninteracting nanoparticles is at ( $t_b/k=0.13$ ).

blocking temperature ( $t_b/k=0.13$ ). The blocking temperature ( $t_b$ ) for the noninteracting ( $g=0$ ) nanoparticles has been obtained as the temperature above which the remanence of the sample is smaller than  $\sim 1\%$ . We should mention at this point that the absence of true spin dynamics in the Metropolis MC simulation algorithm causes the lack of a physical time scale in the algorithm and consequently “time” is measured in MC steps. The observation time in our simulations is  $10^4$  MC steps per spin and corresponds to a physical time of  $t_{MC} \sim 100$  ns (Ref. 30) for noninteracting nanoparticles. This is much shorter than a typical magnetometry observation time  $t_{obs} \sim 100$  s and consequently a much higher blocking temperature is predicted by our simulations ( $T_b \approx K_1 V / 7.7 k_B$ ) than the typical experimental value ( $T_b \approx K_1 V / 25 k_B$ ). However, Metropolis MC simulations mimic efficiently the role of thermal fluctuations and they reproduce qualitatively the trend of the experimental data as a function of temperature.<sup>30</sup>

For noninteracting nanoparticles with random anisotropy, the well known result for the remanence at zero temperature ( $M_r/M_s=0.5$ ) is reproduced. For interacting nanoparticles an increase of the remanence with coupling strength is seen. This trend is dictated by the ferromagnetic character of the dipolar interactions on a hexagonal lattice, which also leads to ferromagnetic long range ordering at the ground state, as has been previously demonstrated by various authors.<sup>9,12–15</sup> In addition, interactions cause a collective reversal of the magnetic moments under an applied field, and as a conse-

quence of that, the coercive field decreases with the dipolar strength. The effects of dipolar interactions can also be observed in the MR curves. In particular, the maximum TMR effect ( $H_{max}$ ) occurs at the coercive field ( $H_{max}=H_c$ ) and a clear downshift of the TMR peak position with increasing dipolar strength is observed. The remanent TMR value decreases with interactions, which is explained by the fact that the TMR value is a measure of the misalignment of the magnetic moments in the system. The FM character of dipolar forces in the hexagonal lattice enhances the alignment of the moments at zero field and consequently reduces the corresponding TMR value.

Next, let us comment on the sensitivity of the MR curve; namely, the absolute value of the slope with respect to the applied field. In the weak coupling regime ( $g/k \leq 0.2$ ) an increase of the sensitivity with increasing dipolar strength is observed, both below and above the coercive field. The same trend is followed by the field-dependent susceptibility in the magnetization curves. The underlying physical mechanism that emerges from the above results is that in the weak coupling limit, the moments rotate almost incoherently to the applied field, with dipolar interactions acting as a perturbation that partially aligns them during rotation. Under reduction of the applied field from negative saturation along the  $x$  axis, dipolar interactions tend to align the moments along the negative  $x$  axis until the field reaches a large positive value enough to overcome the anisotropy barrier. Above this value, reversal of the moments is obtained and the interactions again facilitate the alignment of the moments along the positive  $x$  axis. Thus, the TMR sensitivity is enhanced both in the rise and the fall of the TMR curves. When the dipolar coupling increases the alignment of the moment during rotation becomes more efficient and eventually, in the strong coupling regime ( $g/k \sim 1$ ), dipolar interactions dominate the rotation process and they induce a collective rotation of the moments, which causes an abrupt change of the magnetization at the coercive field and the suppression of the TMR signal. The data in Fig. 2 show that below the blocking temperature, the anisotropy is the dominant mechanism determining the position and value of the TMR peak, even when it is comparable to the dipolar strength ( $g/k \sim 1$ ), while interactions modify mainly the sensitivity. On the other hand, above the blocking temperature (Fig. 3), the sensitivity of TMR is not a monotonic function of the dipolar strength, but it increases with dipolar strength for  $g/k \leq 0.3$  and it decreases for  $g/k \geq 0.3$ , followed by a suppression of the overall TMR signal. In the high-temperature regime, the anisotropy does not play any role and the observed behavior of the TMR signal is due solely to the collective rotation of the nanoparticles driven by dipolar interactions. The decrease of sensitivity occurs mainly because of the strong suppression of the TMR effect.

Finally, a comment on the role of boundary conditions. The trends of the magnetization and TMR shown in Fig. 2 remain unchanged when free boundaries in the  $x$  and  $y$  directions are assumed, provided that the dipolar coupling is weak ( $g/k \leq 0.2$ ), which is the case corresponding to the most common transition metal (Fe, Co) nanoparticles. For stronger coupling ( $g/k \geq 0.3$ ), demagnetization effects

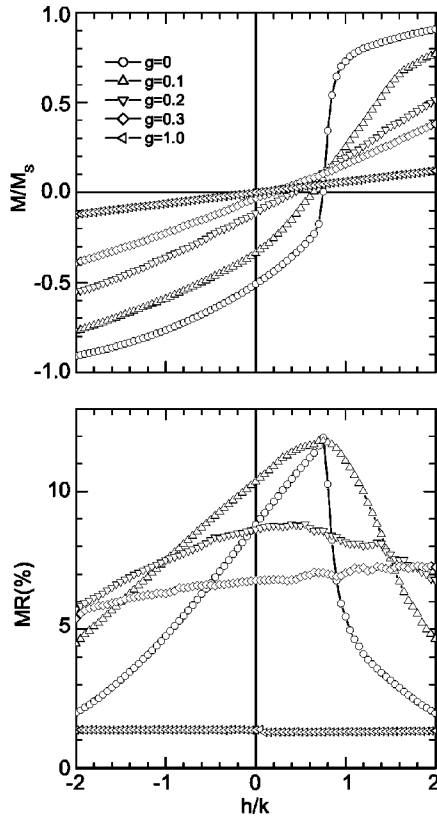


FIG. 4. Low-temperature ( $t/k=0.02$ ) magnetization and TMR for a normal-to-plane ( $z$  axis) magnetic field and various dipolar strengths. Only the lower hysteresis branch is shown.

modify the magnetic structure of the sample and, correspondingly, the TMR curve. As a general characteristic, we have seen that free boundaries lead to a slightly broader TMR peak around the reversal field, arising from a wider local field distribution introduced by the free sample boundaries.

## 2. Normal-to-plane magnetic field

A more dramatic dependence of the magnetic properties on the dipolar strength is expected for an applied field normal to the plane of the array, because dipolar interactions favor the in-plane ordering of the moments, while the applied field drives the moments normal to the plane. The competition between these two orthogonal energy contributions is revealed in the strong dependence of the magnetic properties on the dipolar strength (Fig. 4). With increasing dipolar strength, both the remanence and the coercivity are reduced and the hysteretic behavior of the sample is gradually suppressed and eventually lost in the strong coupling regime ( $g/k \sim 1.0$ ). Correspondingly, the sensitivity of the TMR curve is constantly reduced with increasing coupling strength, and the saturation field increases.

The competition between the in-plane anisotropy (induced by the dipolar interactions) and the normal-to-plane applied field is best seen in the infinite coupling limit ( $g=1, k=0$ ) shown in Fig. 5. In this case the system is anhysteretic because the applied field is normal to the easy plane. At low

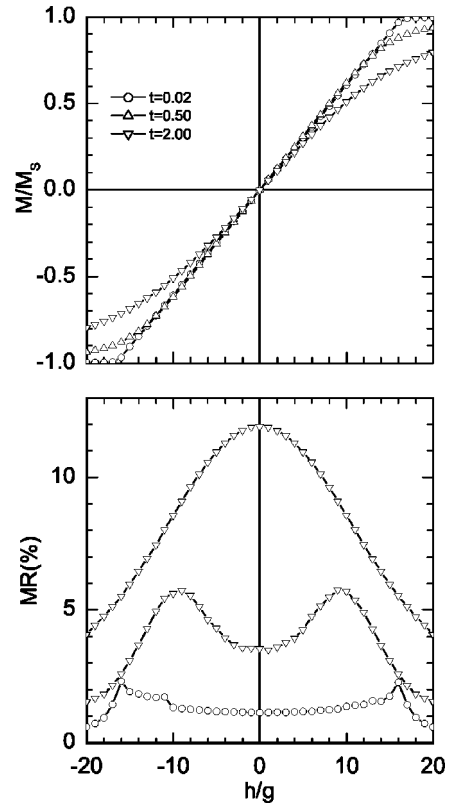


FIG. 5. Magnetization and TMR for dipolar coupled isotropic ( $k=0$ ) nanoparticles for temperatures close to zero ( $t/g=0.02$ ), below the ferromagnetic transition ( $t/g=0.5$ ), and above the ferromagnetic transition ( $t/g=2.0$ ). The magnetic field is normal to the plane along the  $z$  axis.

temperature ( $t/g=0.02$ ), the magnetization curve increases linearly with the field until the value  $h/g \approx 16.5$ , when saturation of the moments along the field is achieved. This is a critical field for saturation normal to the plane, as can be verified by the following argument. Consider the low-temperature magnetization process. At zero field, the dipoles located on a hexagonal lattice in the  $xy$  plane are in their ground state; namely, they are FM ordered along the  $x$  axis (Fig. 1). Upon application of an external field along the  $z$  axis, the dipoles rotate coherently in the  $xz$  plane and the moments assume the form  $\mu_i = \mu(\sin \theta, 0, \cos \theta)$ , where  $\theta$  is the azimuth angle of the dipoles. The total energy of the system is then given by the expression

$$E = -Nh \cos \theta + \frac{1}{2}Ng \left( \sum_i \frac{1}{(r_i/d)^3} - 3 \sin^2 \theta \sum_i \frac{x_i^2}{(r_i/d)^5} \right). \quad (8)$$

The critical field ( $h_0$ ) for irreversible rotation of the moments is obtained from the requirement that the first and second derivatives of the total energy are equal to zero. The second term of the sum in Eq. (8) can be numerically calculated<sup>12</sup> and is equal to  $+5.51709$ , while the term containing the first sum makes a constant contribution to the energy and is irrelevant to the critical field. After some simple algebra,<sup>31</sup> one

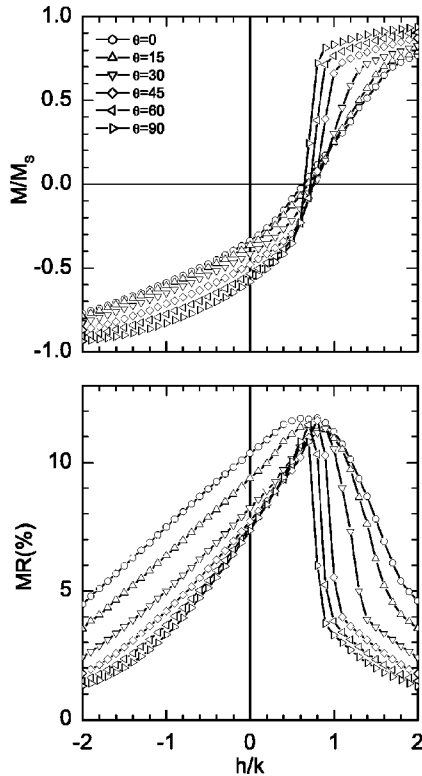


FIG. 6. Variation of the low-temperature ( $t/k=0.02$ ) magnetization and TMR curves with the direction of the magnetic field relative to the  $z$  axis (azimuth). The field is rotated within the  $xz$  plane. The nanoparticles are weakly coupled ( $g/k=0.1$ ).

obtains  $h_0/g=3b \approx 16.551$ , which is in very good agreement with the simulation results in Fig. 5.

With increasing temperature ( $t/g=0.5$ ) the critical field is reduced and the transition to saturation is rounded due to thermal fluctuations. As expected, moment disorder is maximized close to the critical field, and consequently the TMR signal shows a peak around this field. This peak is rather weak at very low temperature ( $t/g=0.02$ ) because the moments rotate coherently. As temperature rises ( $t/g=0.5$ ), thermal fluctuations of the moments are introduced and a double-peak structure of the TMR develops. With further increase of temperature ( $t/g=2.0$ ), the pair of peaks merges to a single one occurring at zero field. The single-peak behavior of TMR indicates that the system is above the critical temperature for dipolar-induced FM ordering.

## B. Dependence of magnetization and TMR on the magnetic field direction

### 1. Variation of the azimuth angle of the magnetic field

The variation of the magnetization and TMR at low temperature ( $t/k=0.02$ ) with the azimuth angle ( $\theta$ ) of the magnetic field for an assembly with weak dipolar coupling ( $g/k=0.1$ ) is shown in Fig. 6 and for moderate coupling ( $g/k=0.2$ ) in Fig. 7. The applied field remains in all cases, shown in Figs. 6 and 7 within the  $xz$  plane ( $\phi=0$ ). The most important feature in these plots is the *large* decrease of the

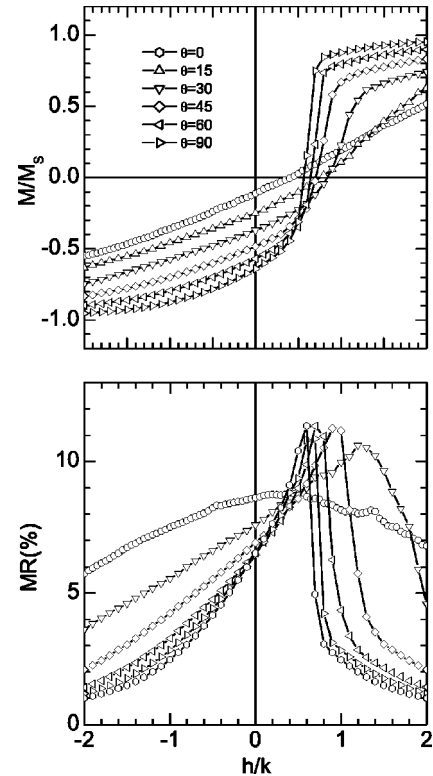


FIG. 7. Variation of the high-temperature ( $t/k=0.02$ ) magnetization and TMR curves with the direction of the magnetic field relative to the  $z$  axis (azimuth). The field is rotated within the  $xz$  plane. The nanoparticles have moderate dipolar strength ( $g/k=0.2$ ).

TMR sensitivity as the magnetic field approaches the  $z$  axis. This trend is clearly seen even in the weak interaction regime (Fig. 6). The strong dependence of the TMR curve on the azimuth angle arises from the competition between the in-plane anisotropy due to interactions and the off-plane direction of the field. In particular, when an in-plane ( $x$  axis) field is gradually reversed, dipolar interactions decrease the TMR sensitivity by introducing an effective anisotropy barrier to in-plane rotation of the moments, as discussed earlier. Contrary to this behavior, when the applied field makes an angle with the  $xy$  plane, it acts against the Lorentz field that favors the in-plane alignment of the moments. Consequently, the saturation field is much higher and the TMR sensitivity is reduced. For weakly coupled nanoparticles (Fig. 6), the rotation of the moment is governed by the anisotropy energy, as deduced from the almost constant value of the coercive field and the TMR peak with the field direction. For moderate coupling (Fig. 7), however, not only the sensitivity decreases more dramatically as the azimuth decreases, but a shift of the coercivity and the TMR peak is seen. A new feature that occurs for moderate coupling (Fig. 7) is that the field corresponding to the TMR maximum ( $h_{max}$ ) can be greater than the coercive field ( $h_c$ ), as occurs for an applied field with azimuth  $\theta=15^\circ$ . The appearance of the TMR peak in hexagonal arrays of nanoparticles at a field higher than the coercive field is in contrast to the commonly met situation in random assemblies of interacting nanoparticles (granular solids), in which the maximum signal is observed at the coer-

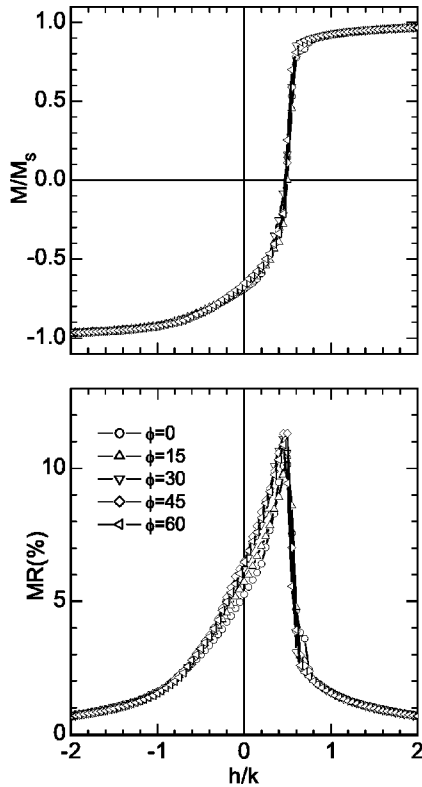


FIG. 8. Weak variation of the magnetization and TMR curves with the in-plane direction of the applied magnetic field. The temperature is low ( $t/k=0.02$ ) and the nanoparticles are coupled with moderate dipolar strength ( $g/k=0.2$ ).

cive field. As discussed above, in the case of a normal-to-plane magnetic field (Fig. 5), strong dipolar forces can suppress the hysteretic behavior and introduce a critical field at which a TMR peak is observed. Taking this idea one step further, we suggest that the occurrence of a TMR peak is associated with a critical field rather than with the coercive field. We deduce from the TMR data shown in Fig. 7 that for directions close to the normal ( $\theta=0^\circ$ ) or close to the plane ( $\theta=90^\circ$ ), the critical field is close to the coercive, but the deviation between the two is maximum around  $\theta=15^\circ$ . The mechanism producing the deviation between the critical and the coercive field is generated by the competition between the three types of energies occurring in the two-dimensional nanoparticle array and the different configurations that they favor: the Zeeman energy that favors alignment along the external field, the dipolar interactions that favor in-plane alignment, and anisotropy that favors random alignment.

## 2. Variation of the polar angle of the magnetic field

Dipolar interactions in a hexagonal lattice induce an in-plane anisotropy with three equivalent easy axes that coincide with the symmetry axes of the lattice. The presence of three equivalent in-plane easy axes reduces the anisotropy barriers for in-plane rotation of the moments and renders the system weakly anisotropic to in-plane rotations of the magnetization. In Fig. 8 we plot the magnetization and TMR for various values of the polar angle ( $\phi$ ) and for moderate dipo-

lar coupling ( $g/k=0.2$ ). The TMR curves for different in-plane directions of the applied field nearly overlap, underlining the weak anisotropy of the sample to in-plane rotations of the moments. It is only in the strong coupling limit  $g/k \sim 1$  (not shown here) that the in-plane anisotropy is dominant and vortices form during reversal of the magnetization, giving rise to steps in the hysteresis curve and to jumps in the TMR curve.

## IV. DISCUSSION

Dipolar interaction effects on the MR have been extensively studied experimentally<sup>32</sup> and theoretically<sup>33</sup> in magnetic granular metals, which typically consist of a random assembly of magnetic nanoparticles in a metallic or insulating matrix. Comparing the present results with those for granular metals, we could say that the most interesting difference between these two systems, is that *in self-assembled arrays, an increase of the field sensitivity to an in-plane field can be achieved by increasing the surface coverage* [ $c \sim (D/d)^2 \sim g^{2/3}$ ], in contrast to what has been known for random assemblies when the packing density [ $x \sim (D/d)^3 \sim g$ ] is increased. We attribute this feature to the ferromagnetic character of the dipolar interactions on the hexagonal lattice, which induce a collective in-plane rotation of the moments. For a normal field, however, the trend of the sensitivity follows that of random assemblies and is reduced with increasing coverage. Given that adjustment of the surface coverage can be experimentally achieved by suitable choice of the capping groups surrounding each nanoparticle,<sup>34</sup> we would expect that changes in the TMR signal with variation of surface coverage could be observed.

In recent experiments, Black *et al.*<sup>2</sup> have measured the TMR effect in self-assembled Co nanoparticle arrays. Small samples of about  $10 \times 10$  nanoparticles were used to measure the magnetoresistance under an in-plane magnetic field. In these measurements, a rich structure in the field-dependent TMR signal was observed and the authors attributed it to the details of the magnetization reversal mechanism. Our simulations with an in-plane magnetic field (Fig. 2) and for  $g/k \sim 0.1-0.2$  correspond to the parameters used in the experiments of Black *et al.*<sup>2</sup> Our results for the hysteresis curves are in good agreement with these experiments. Namely, a remanence value around  $M_r/M_s \sim 0.5$  is found and smooth curves are predicted even for interacting samples, in accordance with these experiments. Our simulated field-dependent TMR curves (Fig. 2) share the same overall characteristics with the corresponding experimental curves;<sup>2</sup> namely, the sharp peak around the coercive field and the asymmetry of the rising and falling parts of the curve. However, no evidence of fine structure in the TMR signal is found, at least within our approach, that treats exactly the magnetic moment correlations within the coherent rotation model. Atomic scale modeling of the magnetic structure of the nanoparticles, would provide a more detailed description of the surface scattering process of the carriers,<sup>35</sup> and could possibly explain the details of the TMR signal in self-assembled arrays.

In conclusion, we have studied the field dependence of the magnetization and tunneling magnetoresistance in a hexago-

nal array of dipolar interacting magnetic nanoparticles with random anisotropy. We showed that for an in-plane applied field, increase of the surface coverage (decrease of interparticle distance) increases the sensitivity of the TMR, through enforcement of the interparticle dipolar interactions, whereas with normal-to-plane field, the opposite effect is achieved. We demonstrated the occurrence of peaks in the TMR associated with a critical field for the reversible-irreversible transition, which are pronounced for strongly interacting dipolar particles ( $g/k > 0.2$ ), and an applied magnetic field around the normal-to-plane direction. Finally, the TMR signal is more sensitive to variations of the azimuth angle of the field rather than the polar angle. As a final remark, our simulations

suggest that magnetoresistance measurements in ordered nanoparticle arrays, as those prepared by self-assembly, could shed light onto the magnetization reversal mechanism and facilitate the quantification of the particle interaction strength.

#### ACKNOWLEDGMENTS

One of the authors (D.K.) acknowledges discussions with Prof. Sir R. J. Elliot and a visiting grant by the Royal Society. This work has been supported by the GROWTH Project No. G5RD-CT-2001-00478.

\*Electronic address: dkehrakos@ims.demokritos.gr

- <sup>1</sup>C. Petit, A. Taleb, and M. P. Pileni, *Adv. Mater.* (Weinheim, Ger.) **10**, 259 (1998).
- <sup>2</sup>C. T. Black, C. B. Murray, R. L. Sandstrom, and S. Sun, *Science* **290**, 1131 (2000).
- <sup>3</sup>V. F. Puentes, K. M. Krishnam, and A. P. Alivisatos, *Appl. Phys. Lett.* **78**, 2187 (2001); *Science* **291**, 2115 (2001).
- <sup>4</sup>G. A. Held, G. Grinstein, H. Doyle, S. Sun, and C. B. Murray, *Phys. Rev. B* **64**, 012408 (2001).
- <sup>5</sup>X. X. Zhang, G. H. Wen, G. Xiao, and S. Sun, *J. Magn. Magn. Mater.* **261**, 21 (2003).
- <sup>6</sup>F. Luis, F. Petroff, J. M. Torres, L. M. García, J. Bartolomé, J. Carrey, and A. Vaurès, *Phys. Rev. Lett.* **88**, 217205 (2002).
- <sup>7</sup>C. B. Murray, S. Sun, H. Doyle, and T. Betley, *MRS Bull.* **26**, 985 (2001).
- <sup>8</sup>S. I. Woods, J. R. Kirtley, S. Sun, and R. H. Koch, *Phys. Rev. Lett.* **87**, 137205 (2001).
- <sup>9</sup>V. Russier, C. Petit, J. Legrand, and M. P. Pileni, *Phys. Rev. B* **62**, 3910 (2000).
- <sup>10</sup>P. Poddar, T. Telem-Shafir, T. Fried, and G. Markovich, *Phys. Rev. B* **66**, 060403 (2002).
- <sup>11</sup>R. L. Stamps and R. E. Camley, *Phys. Rev. B* **60**, 11 694 (1999).
- <sup>12</sup>V. Russier, *J. Appl. Phys.* **89**, 1287 (2001).
- <sup>13</sup>D. Kechrakos and K. N. Trohidou, *Appl. Phys. Lett.* **81**, 4574 (2002).
- <sup>14</sup>P. J. Jensen and G. M. Pastor, *New J. Phys.* **5**, 68 (2003).
- <sup>15</sup>P. Politi and M. G. Pini, *Phys. Rev. B* **66**, 214414 (2002).
- <sup>16</sup>X. Portier, E. Y. Tsybal, and A. K. Petford-Long, *Phys. Rev. B* **58**, R591 (1998).
- <sup>17</sup>S. P. Li, A. Samad, W. S. Lew, Y. B. Xu, and J. A. C. Bland, *Phys. Rev. B* **61**, 6871 (2000).
- <sup>18</sup>C. Tiusan, T. Dimopoulos, K. Ounadjela, M. Hehn, H. A. M. van den Berg, V. da Costa, and Y. Henry, *Phys. Rev. B* **61**, 580 (2000).
- <sup>19</sup>M. Kläui, C. A. F. Vaz, J. Rothman, J. A. C. Bland, W. Wernsdorfer, G. Faini, and E. Cambril, *Phys. Rev. Lett.* **90**, 097202 (2003).
- <sup>20</sup>J. I. Gittleman, Y. Goldstein, and S. Bozowski, *Phys. Rev. B* **5**, 3609 (1972).
- <sup>21</sup>J. S. Helman and B. Abeles, *Phys. Rev. Lett.* **37**, 1429 (1976).
- <sup>22</sup>N. Wiser, *J. Magn. Magn. Mater.* **159**, 119 (1996).
- <sup>23</sup>J. Inoue and S. Maekawa, *Phys. Rev. B* **53**, R11 927 (1996).
- <sup>24</sup>M. Julliere, *Phys. Lett.* **54A**, 225 (1975).
- <sup>25</sup>K. Binder and D. W. Heermann, *Monte Carlo Simulation in Statistical Physics*, in Springer Series in Solid-State Sciences Vol. 80 (Springer, Berlin, 1988), p. 23.
- <sup>26</sup>A. Grzybowski, E. Gwózdź, and A. Bródka, *Phys. Rev. B* **61**, 6706 (2000); E. Lomba, F. Lado, and J. J. Weiss, *Phys. Rev. E* **61**, 3838 (2000); G. T. Gao, X. C. Zeng, and W. Wang, *J. Chem. Phys.* **106**, 3331 (1997).
- <sup>27</sup>R. Meservey and P. M. Tedrow, *Phys. Rev. B* **7**, 318 (1973).
- <sup>28</sup>P. N. Butcher, K. J. Hayden, and J. A. McInnes, *Philos. Mag.* **36**, 19 (1977).
- <sup>29</sup>W. H. Press, S. A. Teukolsky, W. T. Vetterling, and B. P. Flannery, *Numerical Recipes* (Cambridge University Press, 1992), Vol. 1, p. 34; <http://lib-www.lanl.gov/numerical/>
- <sup>30</sup>D. A. Dimitrov and G. A. Wysin, *Phys. Rev. B* **54**, 9237 (1996).
- <sup>31</sup>See, for example, S. Chikazumi, *Physics of Magnetism* (Wiley & Sons, New York, 1964), p. 281.
- <sup>32</sup>J. Q. Xiao, J. S. Jiang, and C. L. Chien, *Phys. Rev. Lett.* **68**, 3749 (1992); P. Allia, M. Knobel, P. Tiberto, and F. Vinai, *Phys. Rev. B* **52**, 15 398 (1995); S. Sankar, A. E. Berkowitz, and David J. Smith, *ibid.* **62**, 14 273 (2000).
- <sup>33</sup>D. Kechrakos and K. N. Trohidou, *Phys. Rev. B* **58**, 12 169 (2000); Y. G. Pogorelov, M. M. P. de Azevedo, and J. B. Sousa, *ibid.* **58**, 425 (1998); D. Kechrakos and K. N. Trohidou, *ibid.* **62**, 3941 (2000); J. V. Lopes, J. M. B. L. dos Santos, and Y. G. Pogorelov, *ibid.* **66**, 064416 (2002).
- <sup>34</sup>S. Sun, C. B. Murray, D. Weller, L. Folks, and A. Moser, *Science* **287**, 1989 (2000).
- <sup>35</sup>Z. Huang, Z. Chen, K. Peng, D. Wang, F. Zhang, W. Zhang, and Y. Du, *Phys. Rev. B* **69**, 094420 (2004).